UC Irvine
UC Irvine Previously Published Works

Title

Altered Function of the SCN1A Voltage-gated Sodium Channel Leads to γ-Aminobutyric Acid-ergic (GABAergic) Interneuron Abnormalities*

Permalink

https://escholarship.org/uc/item/94q9k6xz

Journal

Journal of Biological Chemistry, 285(13)

ISSN

0021-9258

Authors

Martin, Melinda S
Dutt, Karoni
Papale, Ligia A
et al.

Publication Date

2010-03-01

DOI

10.1074/jbc.m109.078568

Peer reviewed

Altered Function of the *SCN1A* Voltage-gated Sodium Channel Leads to γ-Aminobutyric Acid-ergic (GABAergic) Interneuron Abnormalities*[S]

Melinda S. Martin[‡1], **Karoni Dutt**[§1,2], **Ligia A. Papale**[‡¶3], **Céline M. Dubé**[‖**], **Stacey B. Dutton**[‡], **Georgius de Haan**[‡‡], **Anupama Shankar**[‡], **Sergio Tufik**[¶4], **Miriam H. Meisler**[‡‡], **Tallie Z. Baram**[‖**], **Alan L. Goldin**[§‖5], and **Andrew Escayg**[‡6]

From the ‡*Department of Human Genetics, Emory University, Atlanta, Georgia 30322, the Departments of* §*Microbiology and Molecular Genetics,* ‖*Anatomy and Neurobiology, and* ****Pediatrics, University of California, Irvine, California 92697, the* ¶*Department of Psychobiology, Universidade Federal de São Paulo, São Paulo 04024-000, Brazil, and the* ‡‡*Department of Human Genetics, University of Michigan, Ann Arbor, Michigan 48109*

Voltage-gated sodium channels are required for the initiation and propagation of action potentials. Mutations in the neuronal voltage-gated sodium channel *SCN1A* are associated with a growing number of disorders including generalized epilepsy with febrile seizures plus (GEFS+),[7] severe myoclonic epilepsy of infancy, and familial hemiplegic migraine. To gain insight into the effect of *SCN1A* mutations on neuronal excitability, we introduced the human GEFS+ mutation *SCN1A*-R1648H into the orthologous mouse gene. *Scn1a*[RH/RH] mice homozygous for the R1648H mutation exhibit spontaneous generalized seizures and premature death between P16 and P26, whereas *Scn1a*[RH/+] heterozygous mice exhibit infrequent spontaneous generalized seizures, reduced threshold and accelerated propagation of febrile seizures, and decreased threshold to flurothyl-induced seizures. Inhibitory cortical interneurons from P5-P15 *Scn1a*[RH/+] and *Scn1a*[RH/RH] mice demonstrated slower recovery from inactivation, greater use-dependent inactivation, and reduced action potential firing compared with wild-type cells. Excitatory cortical pyramidal neurons were mostly unaffected. These results suggest that this *SCN1A* mutation predominantly impairs sodium channel activity in interneurons, leading to decreased inhibition. Decreased inhibition may be a common mechanism underlying clinically distinct *SCN1A*-derived disorders.

Heterozygous mutations in the neuronal voltage-gated sodium channel gene *SCN1A* are responsible for several disorders including generalized epilepsy with febrile seizures plus (GEFS+),[7] severe myoclonic epilepsy of infancy (SMEI), and familial hemiplegic migraine (1–3). Mutations in *SCN1A* account for ~80% of SMEI cases and 10% of GEFS+ cases. Over half of the more than 600 *SCN1A* mutations in SMEI patients result in protein truncation and loss of function, demonstrating haploinsufficiency of *SCN1A* (4, 5). In contrast, GEFS+ mutations are amino acid substitutions that presumably alter but do not abolish *SCN1A* activity.

The amino acid substitutions R1648H and T875M were the first identified *SCN1A*-GEFS+ mutations (1). The R1648H mutation was identified in a large pedigree with 13 affected members (1). The phenotypes of the R1648H/+ heterozygotes in this family were highly variable and included individuals with only childhood febrile seizures, only afebrile epilepsies such as generalized tonic clonic seizures (GTCS), absence seizures, and myoclonic seizures, and both febrile and afebrile seizures (1). This variation in severity may result from differences in genetic modifiers or environmental influences (4, 6).

GEFS+ families with *SCN1A* mutations have also been identified in which some affected members display neuropsychiatric deficits and ataxia (7, 8). The range of phenotypes among GEFS+ pedigrees that harbor different *SCN1A* mutations suggests that clinical variability may arise from differences in the way the mutations alter Na$_v$1.1 function. However, functional analyses of GEFS+ mutations in heterologous systems have failed to reveal clear genotype-phenotype correlations, and different results have been observed when the same mutation was examined in different expression systems. For example, Na$_v$1.1 channels with the R1648H mutation exhibited faster recovery from inactivation in *Xenopus* oocytes (9) but increased persistent current in HEK cells (10). Both of these effects should increase sodium channel activity. Other GEFS+ mutations (D1886Y and R859C) have been predicted to decrease neuronal

[7] The abbreviations used are: GEFS+, generalized epilepsy with febrile seizures plus; SMEI, severe myoclonic epilepsy of infancy; GTCS, generalized tonic clonic seizures; BAC, bacterial artificial chromosome; ES cell, embryonic stem cell; EEG, electroencephalography; WT, wild type; VPA, valproic acid; MOPS, 4-morpholinepropanesulfonic acid; GABAergic, γ-aminobutyric acid-ergic.

excitability by slowing recovery from inactivation and shifting the voltage dependence of activation or inactivation (11–13).

To examine the *in vivo* effects of *SCN1A* mutations on neuronal function, we first generated transgenic mice that express a bacterial artificial chromosome (BAC) clone containing the mouse *Scn1a* gene into which the R1648H mutation was introduced (14). Electrophysiological analysis of dissociated cortical neurons from the transgenic mice revealed decreased sodium channel function in GABAergic inhibitory interneurons. Recordings from cortical and hippocampal neurons from two *Scn1a* knock-out mouse models of SMEI (15, 16) revealed a similar specific effect of *Scn1a* deficiency in GABAergic interneurons, raising the prospect that impaired inhibitory circuits may be a common feature of disorders that result from *SCN1A* mutations.

To develop a more accurate model of the human disease, we have now introduced the *SCN1A*-R1648H mutation (1, 9) into the mouse genome by homologous recombination at the *Scn1a* locus. Spontaneous generalized seizures in heterozygous ($Scn1a^{RH/+}$) and homozygous ($Scn1a^{RH/RH}$) knock-in mutants as well as the predicted increased susceptibility to experimental febrile seizures were observed. Electrophysiological analysis of dissociated cortical neurons from the knock-in mutants demonstrated delayed recovery from inactivation, increased use dependent inactivation, and reduced action potential firing in inhibitory interneurons, which is predicted to reduce inhibition.

EXPERIMENTAL PROCEDURES

Preparation of the Targeting Construct—The targeting construct consisted of a 4.1-kb 5′ arm of homology, a neomycin cassette flanked by *FLP1* recombinase (Frt) sites, and a 4-kb 3′ arm of homology containing the R1648H mutation and an additional silent substitution resulting in a unique EcoRI site. The final assembled targeting construct was sequenced.

Targeting of the R1648H Mutation to the Mouse Scn1a Gene—The targeting construct was linearized with AvrII, gel-purified, and electroporated into 129X1/SvJ-derived PAT-5 embryonic stem (ES) cells. Six hundred neomycin-resistant clones were selected and screened by PCR amplification for correct targeting of the 3′ arm using the primer pair F4RH (GGAAT AGGAA CTTCG TTCTG CTCG) and R4RH (GTGTG CAACT CTCCC TACCA TAAG). Positive clones were then screened for homologous recombination of the 5′ arm by PCR amplification using the primer pair F5RH (CAAGT GCTAC TTGCC CAGCA G) and R5RH (TTCTG AGGCG GAAAG AACCA G). The PCR reactions were conducted using PCR SuperMix High Fidelity (Invitrogen) under the recommended conditions.

Southern Blot Hybridization—ES cell clones that amplified with both PCR screens were next analyzed by Southern blot hybridization. Ten micrograms of genomic DNA were digested overnight with SpeI, StuI, or BglI and separated by agarose gel electrophoresis. Gels were soaked with agitation in 0.25 M HCl for 10 min, 0.5 M NaOH and 1.5 M NaCl for 20 min, and 1.5 M NaCl and 0.5 M Tris (pH 7.5) for 20 min and then transferred by capillary action to Hybond-XL membranes (Amersham Biosciences) with 10× SSC (1× SSC = 0.15 M NaCl and 0.015 M sodium citrate). Membranes were prehybridized at 65 °C for 2 h

in 7% SDS, 0.25 M Na_2HPO_4 (pH 7.2), and 1 mM EDTA. External probes with homology to the region upstream of the 5′ arm and downstream of the 3′ arm were PCR-amplified with the primer pair 5′F (CAAGC AGAGC TGTTG GCTGA GGT) and 5′R (AGTGT GTAGT TGTAG GTCAT TTGGA GAC) and the pair 3′F (GGACT TCCTA GAATG GCCCC TCAG) and 3′R (CCAAG CGTAA CCATG CTGTA TTTC), respectively. An internal probe with homology to the 5′ arm was amplified using the primer pair 5′intF (CATTA GGAAG GTTTA GATCC ACTG) and 5′intR (CCTAC CTATT CAACC AACCA AAAT). Each probe was radiolabeled with [α-^{32}P]CTP using the Megaprime DNA Labeling System (Amersham Biosciences), purified using MicroSpin G50 columns (Amersham Biosciences), and added to the prehybridization buffer for overnight incubation of the membrane. Membranes were washed twice with 2× SSC and 0.1% SDS, once with 1× SSC and 0.1% SDS, and once with 0.2× SSC and 0.1% SDS at 65 °C for 15 min. Clones identified as correctly targeted were confirmed to have normal karyotypes by chromosome analysis. Southern blot analysis of genomic DNA from tail biopsies of 5-week-old mice was performed as described for the ES cell clones.

Generation of $Scn1a^{RH/+}$ and $Scn1a^{RH/RH}$ Mice—Two clones with the R1648H mutation were injected into blastocysts obtained from mating C57BL/6NCrl female mice with (C57BL/6J X DBA/2J)F1 male mice at the University of Michigan Transgenic Core. Male chimeras with a high percentage of agouti coat color were bred to Tg(ACTFLPe)9205Dym/J females expressing *FLP1* recombinase to test for germ line transmission of the mutation and to delete the neomycin cassette. $Scn1a^{RH/+}$;Tg(ACTFLPe)9205Dym transgene-positive male offspring were bred to C56BL/6J females to produce $Scn1a^{RH/+}$ N1 males. N1 males lacking the FLPe transgene were crossed to C57BL/6J females to create the N2 generation. All experiments on heterozygous mice were conducted at the N2 generation. $Scn1a^{RH/+}$ N2 males and females were crossed to obtain $Scn1a^{RH/RH}$ mice. Mice were maintained at 22 °C on a 12-h light/dark cycle. Food and water were available *ad libitum*. All experiments were performed in accordance with the Institutional Animal Care and Use Committees of Emory University and the University of California, Irvine.

Genotyping of Mutants—To screen for the R1648H mutation, tail DNA was amplified using the *Scn1a*-specific primer pair FRH (TTGAT GACTT CTTCA CTGAT TGAT) and RRH (AGAGG CTCTG CACTT TCTTC). PCR amplification was performed for 32 cycles of 94 °C for 30 s, 55 °C for 30 s, and 72 °C for 45 s. The 591-bp PCR product was digested with EcoRI to distinguish between the wild-type (WT; 591 bp) and mutant (461 bp) alleles. The primers and the PCR conditions provided by The Jackson Laboratory (Bar Harbor, ME) for the B6;SJL-Tg(ACTFLPe)9205Dym/J strain were used to genotype for the presence of the FLPe transgene. To screen for the deletion of the neomycin cassette, tail DNA was amplified with primers flanking the cassette, NeoF (TTTTC AAGTC AGGGT TCCTC), NeoR (GCAGG AAGGG ACATC ATCAG). PCR amplification was performed for 32 cycles of 94 °C for 30 s, 55 °C for 30 s, and 72 °C for 2.5 min. In the presence of the neomycin cassette, a 2.5-kb product was observed, whereas

deletion of the neomycin cassette produced a 767-bp product from the targeted allele.

Northern Blot Analysis—Northern blot analysis was performed on mRNA from the whole brains of 5-week-old mice. Two micrograms of poly(A) RNA was separated by electrophoresis on an agarose gel containing 10% formaldehyde and $1\times$ MOPS. RNA was capillary-transferred with $10\times$ SSC to Hybond-XL membrane (Amersham Biosciences). Membranes were treated as previously described for Southern blot analysis. A published *Scn1a* probe (17) and the DECAtemplate glyceraldehyde-3-phosphate dehydrogenase-mouse probe (Ambion) were radiolabeled, purified, and hybridized as in the Southern blot analysis.

Western Blot Analysis—Western blot analyses from P18 or 5-week-old mouse brains were performed as previously described (18). With each sodium channel antibody, two mice of each genotype were analyzed in duplicate on three separate gels, and protein levels were compared between mutants and wild-type littermates. Briefly, 30–100 μg of protein was separated on 7.5% SDS-polyacrylamide gels and blotted with anti-Na$_v$1.1 (Chemicon, 1:200), anti-Na$_v$1.2 (Alomone, 1:200), anti-Na$_v$1.3 (Alomone, 1:200), or anti-Na$_v$1.6 (Alomone, 1:200) antibodies. Horseradish peroxidase -conjugated goat anti-rabbit secondary antibody (GE Healthcare) was diluted 1:5000. To correct for variation in protein loading, the membrane was also incubated with mouse anti-α-tubulin diluted 1:10,000 (Cedarlane Labs) followed by incubation with horseradish peroxidase-conjugated goat anti-mouse IgG (Jackson ImmunoResearch). Signal was visualized by chemiluminescent detection with the ECL detection system (GE Healthcare), and the intensity of each band was quantified using the Gel Logic 2200 Digital Imaging System (Eastman Kodak Co.) and normalized to the level of α-tubulin.

Kainic Acid Seizure Induction—Kainic acid seizure induction was conducted as previously described (6). Mice between three and six months of age were injected intraperitoneally with 15 or 20 mg/kg kainic acid (Ocean Produce International). Mice were observed for 2 h after the injection of kainic acid and scored according to a modified Racine scale (19).

Flurothyl Seizure Induction—Flurothyl seizure induction was performed as previously described (6). Mice (3–4 months old) were exposed to flurothyl(2,2,2-trifluroethylether) (Sigma) at a rate of 20 μl/min. The latencies to the first myoclonic jerk and to the GTCS were recorded. Progression of the tonic-clonic seizure to tonic hind-limb extension was also noted.

Valproic acid (VPA, Sigma) was dissolved in 0.9% saline and administered at 100, 200, or 300 mg/kg. VPA or saline was injected intraperitoneally 30 min before seizure induction. All experiments were carried out between 12 and 4 p.m. The experimenter was blind to the genotypes of the mice. Male and female data were analyzed separately. There were no observed sex differences in the data; therefore, data from both sexes were combined.

Experimental Febrile Seizure Induction and Analysis—The experimental febrile seizure paradigm was modified from methods published for the rat (20) and adapted to the mouse (21). Briefly, 14–15-day-old mice were exposed to hyperthermia (*i.e.* increased body and brain temperatures) via a warmed air stream. Core temperatures were measured before hyperthermia induction and at the onset of the seizures. The latter were considered threshold temperatures. In addition, the rate of seizure propagation was estimated by examining the progression of phenomenology of the seizure. The onset of experimental febrile seizures usually involves sudden immobility, reduced response to stimulation (altered consciousness), and facial automatisms. These rarely progress to generalized seizures. Because of altered seizure progression in the mutant mice, the latency and threshold temperature to generalized, tonic seizures were also determined. Once threshold and latency were determined, the hyperthermia was discontinued to stop the seizure. All experiments were carried out between 8 a.m. and 1 p.m., and the experimenter was blind to the genotypes.

Electroencephalography—Fourteen *Scn1a*$^{RH/+}$ mice and nine WT littermates (3–5 months old) were implanted for electroencephalography (EEG) recordings as previously described (6). After a minimum of 7 days recovery from surgery, each mouse was placed into a Plexiglas box ($15 \times 15 \times 15$ cm) and attached to a series of bioelectric amplifiers (Embla Somnologica, Iceland) via a small counterbalanced commutator (Dragonfly Research). After 24 h of acclimatization, EEG and electromyography data were collected for 96 h from each mouse, and epileptiform activity was manually scored. Mouse behavior was also simultaneously monitored with digital video recording. Seizures were characterized by polyspike activity accompanied by stereotypic seizure behaviors and a refractory period. Interictal epileptiform activity was characterized by spike discharges that were at least two times the amplitude of the background.

Electrophysiological Recordings—Mice were decapitated after anesthesia with either ice (P5-P10) or halothane (P13-P15), and dissociated cortical neurons were prepared as described previously (22, 23). Excitatory pyramidal neurons and inhibitory bipolar neurons were identified by correlating shape with staining for anti-GluR1 (glutamate receptor 1) (1:5000, Upstate Biotechnology) and anti-GAD67 (glutamic acid decarboxylase 67) (1:5000, Chemicon), respectively (24, 25). Secondary antibodies Alexa Fluor 568-anti-rabbit IgG and Alexa Fluor 488-anti-mouse IgG2a (Molecular Probes) were used for observation with epifluorescent illumination.

Electrophysiological recordings were performed within 24–36 h of obtaining neuronal cultures at 22–25 °C in the whole-cell patch configuration using an Axopatch 200B patch clamp with Digidata 1322A interface and pCLAMP 8 software. The bath solution consisted of 150 mM NaCl, 3 mM KCl, 15 mM tetraethylammonium chloride, 4 mM BaCl$_2$, 0.1 mM CdCl$_2$, and 10 mM HEPES (pH 7.4), and the electrode solution consisted of 140 mM CsF, 10 mM NaCl, 5 mM EGTA, and 10 mM HEPES (pH 7.3). Series resistance was compensated to 80–90%, and linear leak subtraction was used for all recordings. Corrections were made for leak and capacity currents using P/4 subtraction. Currents were filtered at 5 kHz and sampled at 20 kHz.

Current densities were determined in neurons from P13-P15 mice at room temperature (22–25 °C) in voltage clamp mode during a 15-ms depolarization to −5 mV from a holding potential of −70 mV. Series resistance was less than 20 megaohms,

and the current amplitudes were normalized to cellular capacitance. Statistical significance was determined using Student's *t* test.

The voltage dependence of activation and inactivation, recovery from inactivation, and use-dependent inactivation were studied using protocols described by Spampanato *et al.* (9). Briefly, the voltage dependence of activation was analyzed using a protocol with depolarizations from -60 to $+15$ mV in 5-mV intervals. Peak current amplitudes were converted to conductance values, normalized for comparison, and plotted against voltage. The voltage dependence of inactivation was analyzed using varying depolarizations for 50 ms to allow inactivation followed by repolarization and then depolarizing to a test potential of -15 mV to elicit the remaining available current. Peak currents during the test pulse were normalized for comparison and plotted against the voltage of the conditioning pulse. Recovery from inactivation was analyzed using a protocol that first inactivated the channels by depolarization to -5 mV for 50 ms followed by recovery at -80 mV for a variable period of time (2 to 60 ms) and a test pulse to -5 mV. Peak current amplitudes during the test pulse were normalized to peak current amplitudes during the conditioning pulse and plotted against recovery time. Use-dependent inactivation was examined by successive depolarizations to -5 mV from a holding potential of -80 mV at 10 and 39 Hz. Measurement of persistent current was done using prolonged 200-ms depolarizations to -10 mV. Each voltage step was followed by a >5-s recovery period at -80 mV to minimize the accumulation of use-dependent inactivation. Pulse generation, data collection, and analyses were done with pCLAMP 8.0, Excel, and SigmaPlot 9.0 software. Data shown are the means $\pm$ S.E., and statistical significance was determined using Student's *t* test.

The average values of the parameters of activation, inactivation, recovery from inactivation, and use-dependent inactivation shown in Tables 2 and 3 were obtained after fitting the data with the following equations. For activation, $G = 1/(1 + \exp(-0.03937z(V - V_{1/2})))$, in which G is conductance, z is the apparent gating charge, V is the potential of the given pulse, and $V_{1/2}$ is the potential for half-maximal activation. For inactivation, $I = 1/(1 + \exp(V - V_{1/2})/a)$, in which I is equal to the test-pulse current amplitude, V is the potential of the conditioning pulse, $V_{1/2}$ is the voltage for half-maximal inactivation, and a is the slope factor. For recovery: $I = 1 - A\exp(-t/\tau) - c$, in which A is the fraction of current that recovered with the time constant τ, t is the recovery time, and c is the fraction of current that did not recover. For use-dependent inactivation: $I = A_1\exp(-t/\tau) + c$ (single exponential), in which A_1 is the relative fraction of current that decayed with the time constant τ, t is the decay time, and c is the remaining current.

Current-clamp recordings were performed on dissociated cortical neurons from P8-P10 mice within 48 h of culture. Neurons were visualized using infrared differential interference contrast optics and selected based on shape. Recordings were performed at room temperature (22–25 °C) using a Multiclamp 700A patch clamp amplifier and pClamp 10.2 software (Molecular Devices). Signals were sampled at 25 kHz and filtered at 10 kHz. The pipette solution contained 126 mM potassium gluconate, 4 mM KCl, 10 mM HEPES, 4 mM Mg-ATP, 0.3 mM Tris-

GTP, 10 mM phosphocreatine, pH 7.2. The bath solution contained 126 mM NaCl, 1.25 mM NaH$_2$PO$_4$, 2.5 mM KCl, 2 mM CaCl$_2$, 2 mM MgCl$_2$, 26 mM NaHCO$_3$, and 10 mM glucose, pH 7.3. After forming a seal and performing capacitance and series resistance compensations, the passive properties of the cells were recorded in voltage clamp mode. Before switching to current-clamp mode, the resting membrane potential was measured, and only neurons with resting potentials between -55 and -70 mV were used. Firing patterns were recorded in response to 2-s depolarizing current injections in 20-pA increments starting at 10 pA. Hyperpolarizing current in steps of 5-pA decrements was injected to measure the input resistance, and neurons with input resistance of 60–80 megaohms were selected for analysis. The number of action potentials in 2 s was counted, and only over-shooting action potentials more positive than 0 mV were included. Data are represented as the means $\pm$ S.E. Statistical significance was determined using Student's *t* test with $p < 0.05$ as the criterion for significance.

RESULTS

Targeted Insertion of the R1648H Mutation into the Mouse Scn1a Gene—We generated a mouse model of human GEFS+ by knocking in the *SCN1A*-R1648H mutation into exon 26 of the mouse *Scn1a* gene (Fig. 1*A*). This mutation resulted in the substitution of a positively charged arginine residue in the voltage sensor of domain 4 with a histidine residue (1). Six hundred neomycin-resistant ES cell clones were screened for correct targeting by PCR amplification of the 3′ and 5′ regions of homology (Fig. 1*B*). Clones that were positive in both PCR assays were examined by Southern blot analysis. Two correctly targeted ES cell clones were injected into blastocysts to generate chimeric mice that were bred to generate the knock-in mice. The presence of the targeted allele in the resulting lines of mice was confirmed by Southern blot analysis with 5′ and 3′ probes (Fig. 1*C*).

Northern blot analysis of mRNA from the whole brains of $Scn1a^{RH/+}$ mice detected the expected full-length *Scn1a* transcript. The expression level of the *Scn1a* transcript was comparable in heterozygous $Scn1a^{RH/+}$ mutants and WT littermates (Fig. 2*A*). Western blot analysis of protein extracts from the whole brains of P18 $Scn1a^{RH/+}$ and $Scn1a^{RH/RH}$ mutants (Fig. 2*B*) and 5-week-old $Scn1a^{RH/+}$ mutants (Fig. 2*C*) revealed levels of Na$_v$1.1, Na$_v$1.2, Na$_v$1.3, and Na$_v$1.6 that were comparable with WT littermates. Only full-length Na$_v$1.1 protein was detected in the mutants (supplemental Fig. 1). These data demonstrate the *in vivo* stability of the R1648H transcript and the mutant channel protein.

Homozygous Scn1a$^{RH/RH}$ Mutants Exhibit Spontaneous Seizures and Shortened Life Span—$Scn1a^{RH/RH}$ mutants were visually indistinguishable from $Scn1a^{RH/+}$ mice and WT littermates until approximately P16. Beginning at P16, recurrent visible seizures were observed in $Scn1a^{RH/RH}$ mice. The behavioral seizures typically lasted 30–90 s and were characterized by excessive jumping, repetitive jerking of all four limbs, head nodding, and clonus of the forelimbs and tail. Some behavioral seizures ended with hindlimb extension, typical of severe seizures in the mouse. The life span of the $Scn1a^{RH/RH}$ mutants was 16–26 days, with a mean life span of 18.5 days (Fig. 3*A*). The
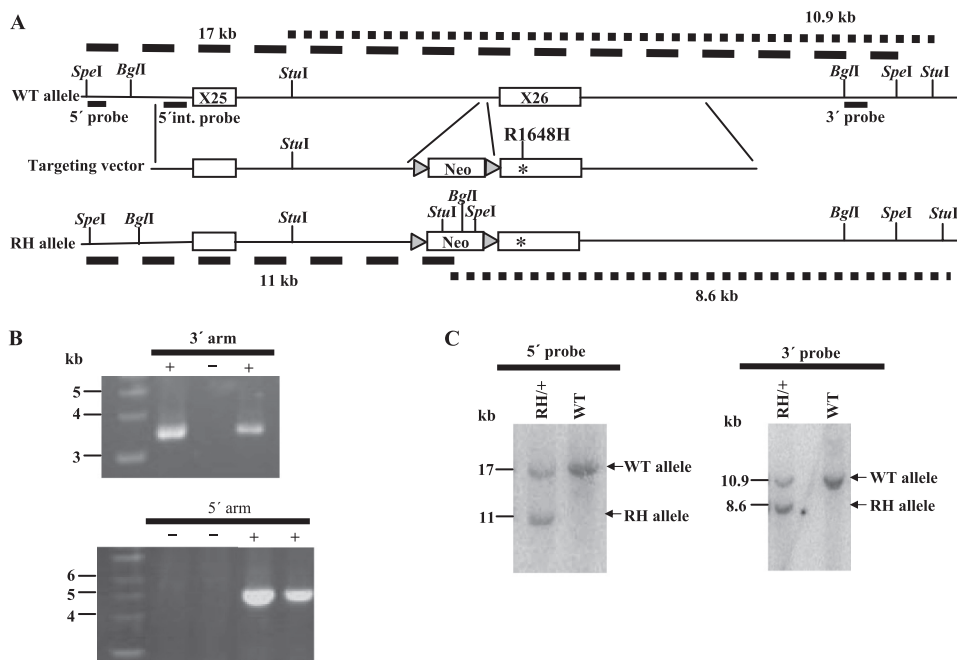
FIGURE 1. **Generation of the *Scn1a* GEFS+ mouse model by targeted knock-in of the human R1648H mutation.** *A*, shown is an illustration of the wild-type *Scn1a* locus, the targeting vector, and the targeted *Scn1a* allele with the R1648H mutation. StuI, SpeI, and BglI restriction sites, the location of probes for Southern blot analysis, and the lengths of the predicted restriction fragments are shown. *B*, PCR screen of neomycin-resistant ES cell clones. +, positive clone; −, negative clone. *C*, Southern blot analysis is shown of genomic DNA from *Scn1a*^RH/+^ and WT mice after digestion with SpeI and StuI. After digestion with SpeI, the 5′ probe detected the expected 17- and 11-kb fragments from the WT and RH allele, respectively. Fragments of 10.9 and 8.6 kb from the WT and RH allele, respectively, were detected with the 3′ probe following digestion with StuI. *RH*, R1648H.

charges that were at least two times the amplitude of the background (Fig. 4*C*). The average duration of the seizures was 32.9 ± 1.8 s. All seizures were associated with stereotypic motor behaviors and were followed by a refractory period with an average length of 62.4 ± 12.7 s. Spontaneous seizures have also been observed in additional *Scn1a*^RH/+^ mutants during routine mouse colony management procedures. Seizures and spike discharges were not observed in the EEG recordings from the WT mice. The observation of spontaneous seizures in only two *Scn1a*^RH/+^ mutants is likely due, in part, to the mixed genetic background and is consistent with the variability observed among affected members of GEFS+ families. A variable incidence of spontaneous seizures was also observed in *Scn1a*^+/−^ mice, with seizures detected in 3 of 7 mutants examined (15).

Scn1a^RH/+^ *Mice Exhibit Reduced Thresholds to Flurothyl-induced and Experimental Febrile Seizures*—To determine whether heterozygosity for the R1648H mutation alters seizure thresholds, we first examined the response to the chemiconvulsant flurothyl. We measured the latency to the myoclonic jerk, the first observable behavioral response, and latency to the GTCS (Fig. 5*A*). We observed no difference in the latency to the myoclonic jerk in *Scn1a*^RH/+^ mutants. However, *Scn1a*^RH/+^ mice exhibited a 19% reduction ($p = 0.02$) in the latency to the GTCS compared with WT littermates, indicating that GEFS+ mice are more susceptible to flurothyl-induced generalized seizures.
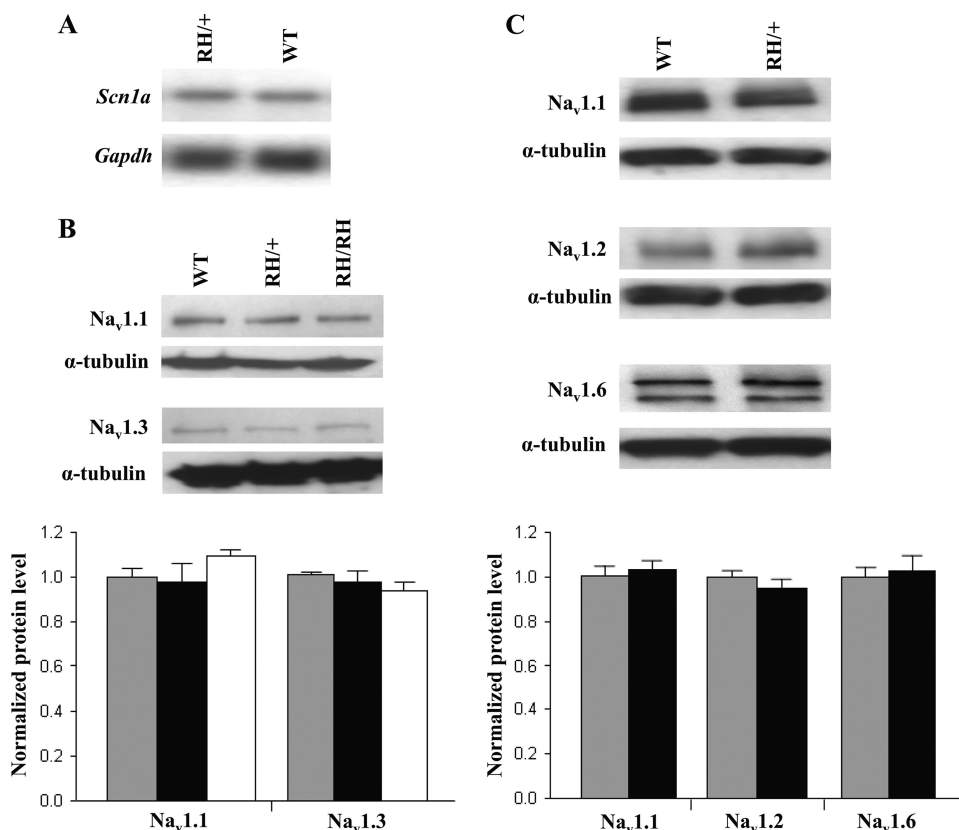
VPA is a broad-spectrum anticonvulsant used in the treatment of GEFS+ patients. We assessed the ability of VPA to correct the increased susceptibility to flurothyl-induced seizures observed in the mutant mice. Serum levels of VPA corresponding to therapeutic levels in humans can be achieved in mice by acute administration of 200 mg/kg VPA (26). Single doses of 100, 200, or 300 mg/kg of VPA or saline control were administered to *Scn1a*^RH/+^ mutants and WT littermates. Thirty minutes after administration of VPA, latency to flurothyl-induced GTCS was measured (Fig. 5*B*). Injection of 200 or 300 mg/kg of VPA returned the latency of *Scn1a*^RH/+^ mutants back to WT values (Fig. 5*B*). The values for latency to GTCS after 200 mg/kg VPA were 9.7 ± 1.2 min in WT mice and 9.2 ± 1.8 min in heterozygous mutants ($p = 0.53$). After 300 mg/kg VPA, the latency was 14.2 ± 3.7 min in WT and 13.1 ± 3.5 min in the mutants ($p = 0.53$).

The seizure thresholds of the *Scn1a*^RH/+^ mice were also examined after the administration of kainic acid at doses of 15 and 20 mg/kg. Seizure progression was determined using a modified Racine scale (19). The response of the heterozygous

phenotype of *Scn1a*^RH/RH^ homozygotes is very similar to homozygous null mice (15, 16), indicating that the R1648H mutation has a more profound effect *in vivo* than suggested by earlier studies in heterologous expression systems.

Before seizure onset, *Scn1a*^RH/RH^ mutants gained weight at a rate similar to *Scn1a*^RH/+^ and WT littermates. From approximately P15, body weight began to decrease, and by P18 the average weight of *Scn1a*^RH/RH^ mice was 23% lower than their littermates ($p = 1.0 \times 10^{-7}$) (Fig. 3*B*). Feeding behavior appeared to be normal, and excessive separation from the dam was rarely observed.

Nissl staining of brain sections from P18 homozygous and five-month-old heterozygous mutants revealed normal brain morphology and no gross reduction in cell density in the hippocampus or cortex compared with WT littermates. Neuronal cell abundance was investigated using the neuron-specific marker NeuN. Neither *Scn1a*^RH/+^ nor the *Scn1a*^RH/RH^ mutants displayed a loss of NeuN immunoreactivity, demonstrating normal neuronal cell viability (data not shown).

Heterozygous Scn1a^RH/+^ *Mutants Exhibit a Low Level of Spontaneous Seizures*—EEG recordings were obtained for a period of 96 h from each of 14 freely moving 3–5-month-old *Scn1a*^RH/+^ mutants (1344 h total) and 9 age-matched WT littermates (864 h total). Generalized seizures were detected in two *Scn1a*^RH/+^ mutants. In these mice a total of 21 spontaneous generalized seizures were recorded during the combined 192 h of EEG analysis. Representative recordings are shown for a wild-type control (Fig. 4*A*) and a heterozygous mutant (Fig. 4, *B* and *C*). The seizures in the *Scn1a*^RH/+^ mutants involved both hemispheres of the brain and were characterized by spike dis-

mutants was not statistically different from their WT littermates at either dose, indicating that the mutation does not increase susceptibility to all forms of seizure induction.

Because febrile seizures are a prominent symptom in patients with the R1648H mutation, we tested whether the knock-in mice also demonstrated increased susceptibility to febrile seizures. This was accomplished by comparing threshold temperatures and the latency to the onset and tonic generalization of these seizures in WT, $Scn1a^{RH/+}$, and $Scn1a^{RH/RH}$ mice. Threshold temperatures for the onset of tonic febrile seizures in $Scn1a^{RH/+}$ and $Scn1a^{RH/RH}$ mutants were significantly lower than those in WT littermates (Fig. 5C, one way analysis of variance, $p = 0.0007$). In addition, the latency to the tonic seizure onset was shorter in $Scn1a^{RH/+}$ and $Scn1a^{RH/RH}$ mutants (Fig. 5D, one way analysis of variance, $p = 0.01$).

GABAergic Interneurons Exhibit Slowed Recovery from Inactivation and Elevated Use-dependent Inactivation in $Scn1a^{RH/+}$ and $Scn1a^{RH/RH}$ Mice—To determine the mechanism by which the R1648H mutation altered neuronal excitability, we examined the electrophysiological properties of dissociated cortical neurons using whole-cell voltage clamp. Neurons were separated into the two major classes of cortical neurons: excitatory pyramidal-shaped neurons and inhibitory bipolar-shaped interneurons. Excitatory pyramidal neurons and GABAergic interneurons were first identified by antibody staining to

FIGURE 2. **Expression of the CNS voltage-gated sodium channels is unaltered in R1648H mutants.** A, Northern blot from $Scn1a^{RH/+}$ and WT littermates revealed comparable expression of the $Scn1a$ transcript. B, Western blot of brain membrane proteins from $Scn1a^{RH/RH}$, $Scn1a^{RH/+}$, and WT littermates at P18 demonstrate normal levels of $Na_v1.1$ and $Na_v1.3$ in the mutants. C, levels of $Na_v1.1$, $Na_v1.2$, and $Na_v1.6$ proteins were comparable in 5-week-old $Scn1a^{RH/+}$ mice and WT littermates. The expected 260-kDa sodium channel α-subunit protein band was detected in all Western blots. Quantitative analysis of protein levels was performed on three separate Western blots. Bar graphs of relative protein levels are shown below the representative Western blots. The amount of each sodium channel protein was normalized against α-tubulin. The ratio from the WT littermates was assigned a value of 1. Gray bars, WT; black bars, $Scn1a^{RH/+}$; white bars, $Scn1a^{RH/RH}$. RH/+, $Scn1a^{RH/+}$; RH/RH, $Scn1a^{RH/RH}$. Error bars represent S.E.
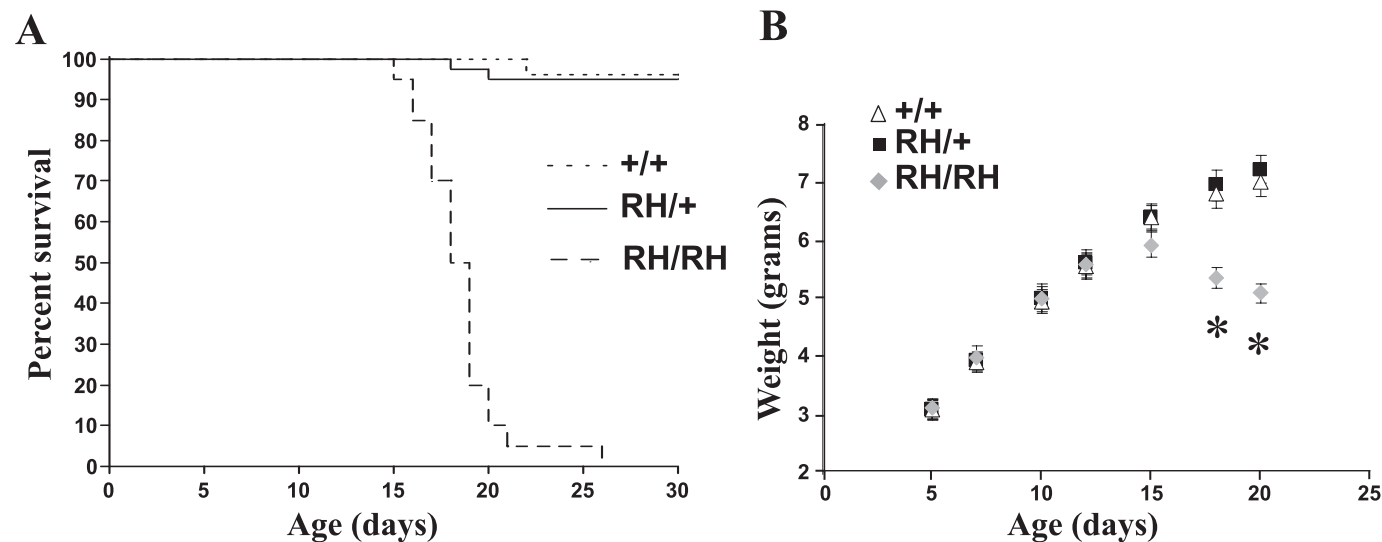
FIGURE 3. **$Scn1a^{RH/RH}$ mutants display shortened life span and reduced body weight.** A, $Scn1a^{RH/RH}$ mutants exhibited a marked reduction in life span; $n = 20–40$ per group. B, the weight gain of $Scn1a^{RH/+}$ mutants and WT littermates are indistinguishable; however, $Scn1a^{RH/RH}$ mutants exhibit a reduction in body weight beginning at P15; $n = 20–34$ per group. *, $p < 0.05$ compared with WT. The values shown are the mean ± S.E.
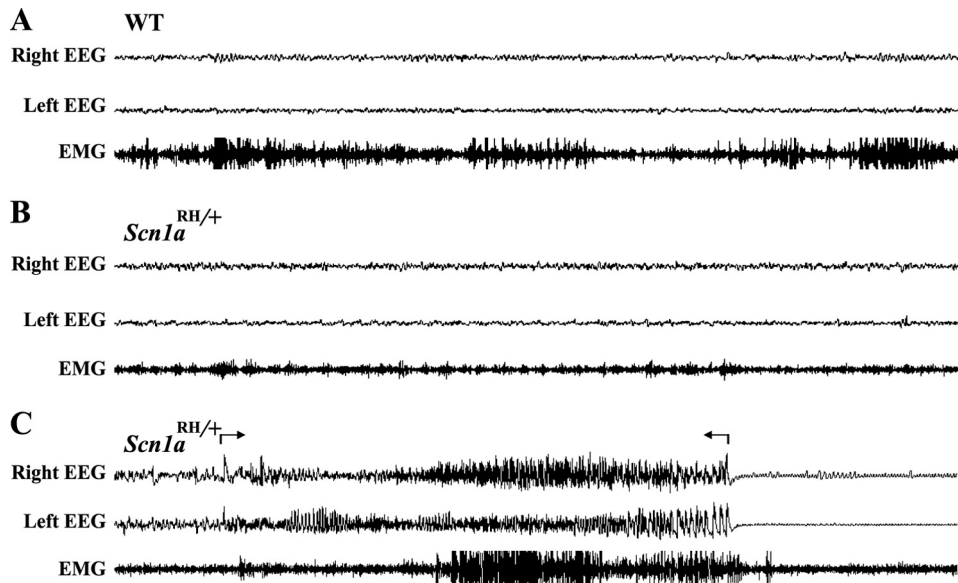
FIGURE 4. **Spontaneous seizure in an *Scn1a^{RH/+}* mouse.** Representative EEG recordings from a five-month-old WT mouse and an *Scn1a^{RH/+}* littermate. *A*, a normal EEG pattern from an awake WT mouse is shown. *B*, a normal EEG pattern from an *Scn1a^{RH/+}* mutant is shown. *C*, an EEG pattern from an *Scn1a^{RH/+}* mutant during an ictal episode. *Arrows* mark the boundaries of a 32-s polyspike discharge in both hemispheres accompanied by muscle activity, as indicated by the electromyography channel. The seizure was followed by a refractory period. *Right EEG*, channel recording from right hemisphere. *Left EEG*, channel recording from left hemisphere; *EMG*, channel recording from neck muscle.
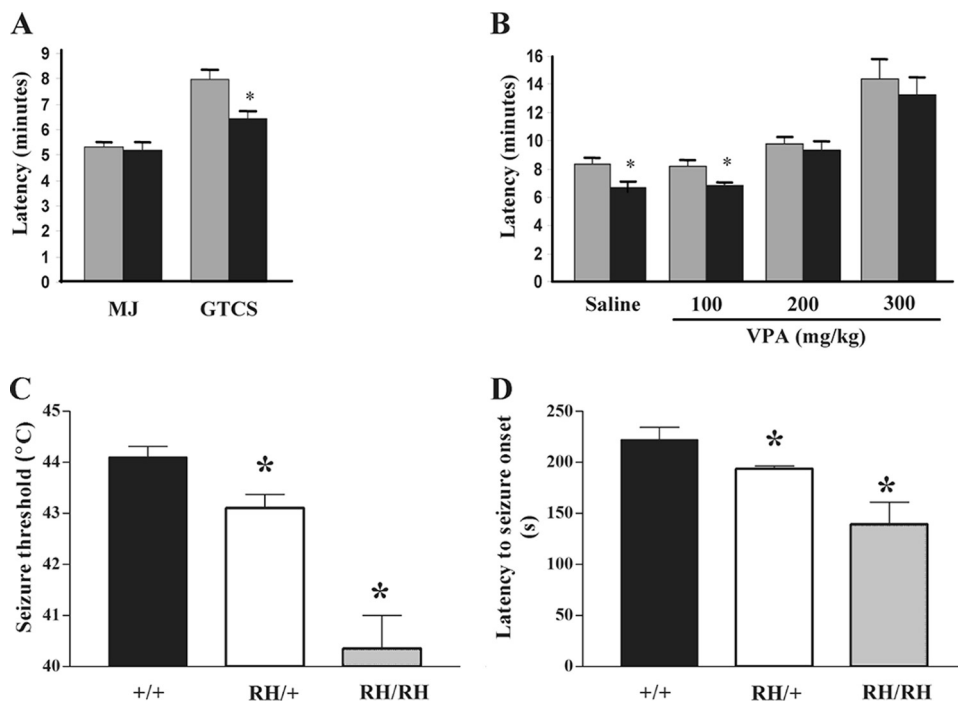

FIGURE 5. ***Scn1a^{RH/+}* mutants exhibit reduced seizure thresholds.** *A*, shown is latency in minutes to the myoclonic jerk (*MJ*) and the GTCS after exposure to flurothyl in *Scn1a^{RH/+}* mutants and WT littermates. *B*, VPA restores normal thresholds to flurothyl-induced seizures in *Scn1a^{RH/+}* mice. Latency in minutes to the GTCS at 100, 200, and 300 mg/kg VPA is shown. *Gray bars*, WT; *black bars*, *Scn1a^{RH/+}*. *, $p < 0.05$ compared with WT. The values shown are the mean ± S.E. *C*, *Scn1a^{RH/+}* and *Scn1a^{RH/RH}* mutants are more susceptible to generation and rapid propagation of experimental febrile seizures compared with WT littermates (+/+). Threshold temperatures for the onset of tonic febrile seizures were significantly lower in *Scn1a^{RH/RH}* (40.4 ± 0.65 °C) and *Scn1a^{RH/+}* mutant mice (43.1 ± 0.26 °C) when compared with WT littermates (44.1 ± 0.21 °C). *, $p < 0.05$, one-way analysis of variance. *D*, latencies to the tonic febrile seizure onset were significantly shorter for the *Scn1a^{RH/+}* mutants mice compared with the WT mice and were further reduced in the *Scn1a^{RH/RH}* mutants. *, $p < 0.05$, one-way analysis of variance.

glutamate receptor 1 (anti-GluR1) and glutamic acid decarboxylase 1 (anti-GAD67), as previously described (14). We then correlated immunostaining with cell morphology to identify bipolar-shaped GABAergic interneurons and pyramidal-shaped excitatory neurons for patch clamping. We examined cortical neurons because of the development of spontaneous generalized seizures in the mutant mice. Representative current traces recorded from bipolar and pyramidal cortical neurons from *Scn1a^{RH/+}*, *Scn1a^{RH/RH}*, and WT littermates at P13-P15 are shown in Fig. 6.

Because it was previously observed that the loss of one sodium channel allele in a mouse model of SMEI leads to a 40% reduction in sodium current in bipolar neurons (15), it was possible that the R1648H GEFS+ mutation could also lead to decreased levels of sodium current. Therefore, we first determined the total sodium current in bipolar neurons and pyramidal neurons from *Scn1a^{RH/+}*, *Scn1a^{RH/RH}*, and WT littermates at P13-P15. To account for differences in cell sizes, the total current was normalized to the cellular capacitance, which is directly proportional to the total quantity of cell membrane. Bipolar neurons from WT mice demonstrated a higher current density than pyramidal neurons, with a ratio of 2.70 (Table 1). The higher density in bipolar neurons is consistent with previous results from an SMEI mouse model (15) and from wild-type mice in which the dendritic sodium current density in interneurons was approximately three times higher than the density in principal neurons (27). In contrast, bipolar neurons from *Scn1a^{RH/+}* and *Scn1a^{RH/RH}* demonstrated a current density than was similar to that of pyramidal neurons, with ratios of 0.94 and 0.95, respectively. There is a trend toward increased current density in pyramidal neurons from *Scn1a^{RH/+}* and *Scn1a^{RH/RH}* compared with WT mice, although these differences were not statisti-
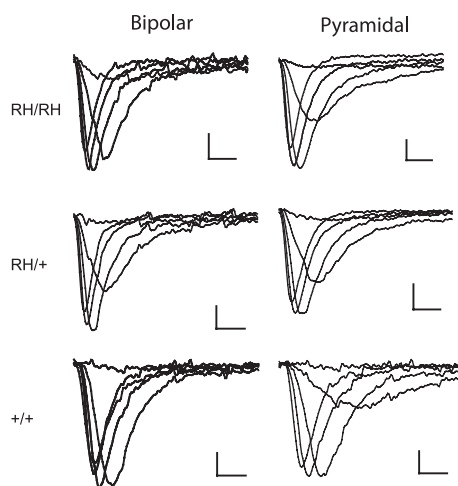
FIGURE 6. **Voltage-clamp traces of sodium currents in dissociated cortical bipolar and pyramidal neurons from P13-P15 mice.** Sodium currents were recorded from a holding potential of −80 mV during depolarizations from −60 to 15 mV in 5-mV steps, although the traces are only shown for depolarizations between −40 and 10 mV in 10-mV steps. *Scale bars* indicate 200 pA and 1 ms.

TABLE 1

Current densities in bipolar and pyramidal neurons

Current densities were determined in neurons from P13–15 mice as described under "Experimental Procedures." The values shown are the mean ± S.E. pF, picofarads.

Genotype	RH/RH	RH/+	WT
Bipolar density (pA/pF)	−83 ± 10[a]	−60 ± 4[a]	−146 ± 29
Bipolar number of cells	12	8	9
Pyramidal density (pA/pF)	−87 ± 14	−64 ± 10	−54 ± 9[a]
Pyramidal number of cells	10	7	7
Current ratio (bipolar/pyramidal)	0.95	0.94	2.70

[a] Statistically significant difference compared to wild-type bipolar neurons ($p < 0.05$).

cally significant. These results indicate that the R1648H mutation specifically decreased the total sodium current amplitude in bipolar neurons.

In addition to the effect on sodium current amplitudes, it was possible that the R1648H mutation might also alter the functional properties of the channel. Previous studies using heterologous systems have reported effects on activation, inactivation, use-dependent inactivation, and percentage of persistent current for this mutation (9, 10, 28). We examined all of these properties in bipolar and pyramidal neurons from $Scn1a^{RH/+}$, $Scn1a^{RH/RH}$, and WT littermates. Neurons were isolated at P13-P15, the oldest age before the $Scn1a^{RH/RH}$ mutants started to die, and at P5-P8, before the onset of seizures when Na$_v$1.1 channels begin to be expressed (16).
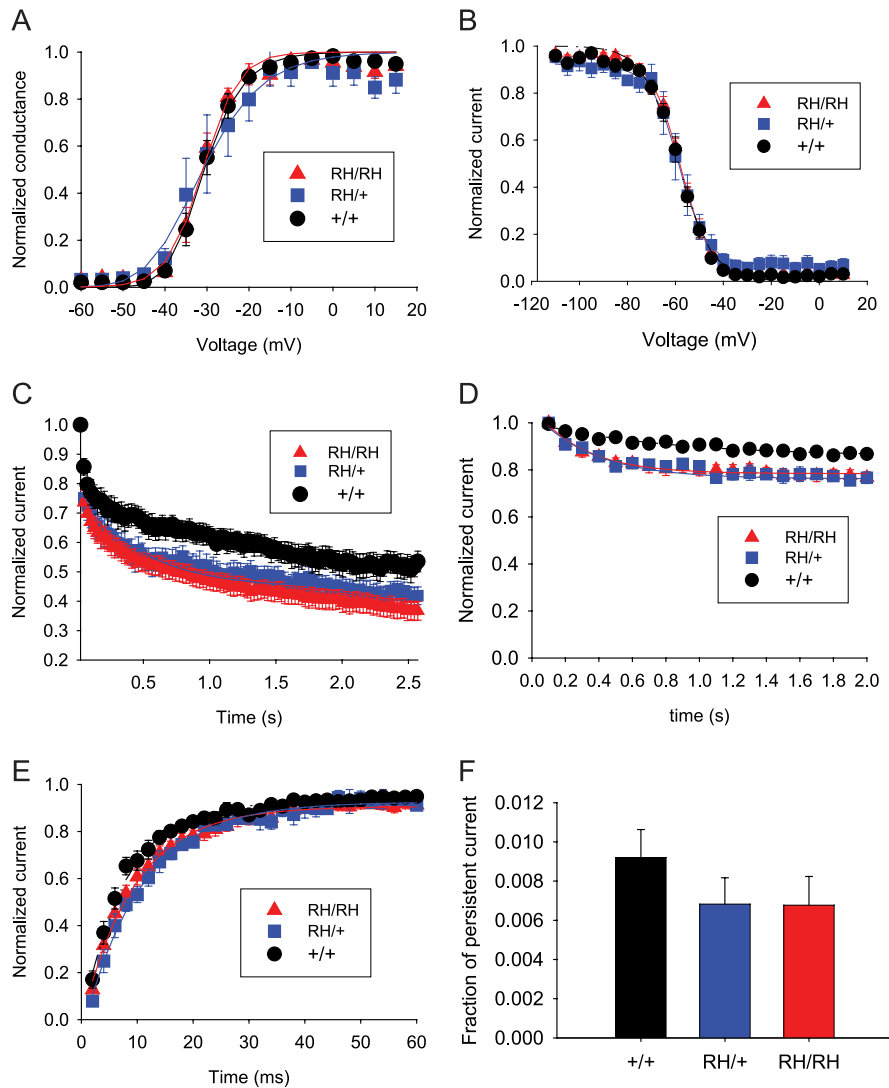
In cortical bipolar neurons from P13-P15 mutant mice, there were no significant differences in the voltage dependence of sodium channel activation or inactivation compared with bipolar neurons from WT mice (Figs. 7, *A* and *B*, Table 2). The most significant difference was increased use-dependent inactivation with rapid stimulation. Use-dependent inactivation refers to the reduction in sodium current that is observed during successive depolarizations when there is insufficient time between depolarizations for the channels to fully recover from inactivation. With repetitive depolarizations at 39 Hz, neurons from $Scn1a^{RH/+}$ and $Scn1a^{RH/RH}$ mice demonstrated a greater decrease in current compared with WT mice (Fig. 7*C*, Table 2).

A less pronounced effect was observed with repetitive depolarizations at 10 Hz, a frequency at which there is only minimal use-dependent inactivation (Fig. 7*D*, Table 2). Consistent with this result, R1648H neurons also demonstrated slower recovery from inactivation (Fig. 7*E*). The time constant for recovery was significantly larger and the extent of recovery was significantly reduced in neurons from homozygous and heterozygous mice (Table 2). Neurons from the mutant mice demonstrated slightly less persistent current, but this difference was not statistically significant (Fig. 7*F*). Similar effects of the R1648H mutation were observed in bipolar neurons from P5-P8 mice (Table 2).

Anti-mGluR1-positive pyramidal-shaped neurons from $Scn1a^{RH/+}$ and $Scn1a^{RH/RH}$ mice showed no significant differences in most of the functional properties examined. Specifically, there were no significant differences in the voltage dependence of activation and inactivation, use-dependent inactivation, or the percentage of persistent current in neurons from either P13-P15 or P5-P8 mice (Table 3). The only significant difference was that the time constant for recovery from inactivation was faster for $Scn1a^{RH/RH}$ compared with WT P13-P15 mice. However, the relevance of this effect is unclear, as no significant differences were observed in use-dependent inactivation at either age, and the difference in recovery time constants was not observed for pyramidal neurons from P5-P8 mice.

GABAergic Interneurons from Scn1a^{RH/RH} Mice Exhibit Decreased Action Potential Firing—To determine whether the electrophysiological differences in sodium channel properties altered neuronal excitability, we measured the number of action potentials in response to 2-s injections of current in 20-pA increments starting at 10 pA. Sample traces of bipolar and pyramidal neurons during current injections from 10 to 110 pA are shown in Fig. 8*A*, and summary data showing the number of action potentials fired during the 2-s interval are shown in Fig. 8*B*. On average, bipolar neurons from WT and heterozygous $Scn1a^{RH/+}$ mice fired comparable numbers of action potentials for all magnitudes of current, reaching a maximum of ∼35 action potentials and then tapering off at the highest levels of current (Fig. 8*B*), although some cells from $Scn1a^{RH/+}$ mice showed reduced firing (Fig. 8*A*). In contrast, bipolar neurons from homozygous $Scn1a^{RH/RH}$ mice reached a maximum of only 20 action potentials when 70 pA was injected, and the number decreased with successively higher current injections.

Pyramidal neurons from all three genotypes fired fewer action potentials, with neurons from WT and heterozygous $Scn1a^{RH/+}$ mice reaching a maximum of ∼20 action potentials before decreasing. Pyramidal neurons from homozygous $Scn1a^{RH/RH}$ mice showed reduced numbers of action potentials at the lowest current injections, with brief bursts at the beginning of the injection (Fig. 8*A*). However, the number of action potentials was comparable with those for neurons from WT and heterozygous $Scn1a^{RH/+}$ mice for current injections above 90 pA, so that it is unclear if the difference at lower levels of current is physiologically significant. In contrast, the markedly reduced action potential firing in bipolar neurons from $Scn1a^{RH/RH}$ mice compared with WT and $Scn1a^{RH/+}$ mice

FIGURE 7. **Electrophysiological recordings show altered sodium channel properties in dissociated corti-cal bipolar neurons from P13-P15 mice.** *A,* no differences in voltage dependence of activation are shown. Sodium currents were recorded from a holding potential of −80 mV during depolarizations from −60 to 15 mV in 5-mV steps, and conductance values were calculated as described under "Experimental Procedures." Data were fit with a single exponential equation. *B,* no differences in voltage dependence of inactivation are shown. The voltage dependence of inactivation was determined using a two-step protocol with conditioning pulses from −110 to 10 mV followed by a test depolarization to −5 mV. The data were fit with a two-state Boltzmann equation. *C,* increased use dependent inactivation at 39 Hz is shown. Currents were elicited by depolarizations to −5 mV from a holding potential of −80 mV at a frequency of 39 Hz. The data were fit with a single expo-nential decay equation. *D,* shown is increased use-dependent inactivation at 10 Hz. Currents were elicited by depolarizations to −5 mV from a holding potential of −80 mV at a frequency of 10 Hz. The data were fit with a single exponential decay equation. *E,* small differences in recovery from inactivation are shown. Currents were elicited with a two-pulse protocol that consisted of a conditioning depolarization to −5 mV for 50 ms followed by a test depolarization to −5 mV, with the recovery time between the two pulses decreasing from 60 to 2 ms. Fractional recovery was determined as described under "Experimental Procedures." The data were fit with a single exponential equation. *F,* no differences in persistent current were shown. Persistent current was deter-mined during a prolonged 200-ms depolarization to −10 mV.

mutant mice developed spontane-ous seizures and weight loss starting at P15, the time when *Scn1a* expres-sion approaches adult levels (16). Generalized seizures were fre-quently observed in the homozy-gous mutants, and these mice had an average life span of 18.5 days. Because severe convulsive seizures may impair the autonomic nervous system and lead to cardiac arrest (29), premature lethality in these mice may be due to severe motor seizures. Consistent with the severe phenotype of homozygous mice, there are no known patients with two mutant *SCN1A* alleles. In addi-tion, *Scn1a*[RH/RH] mutants also dis-play jumping, erratic behavior, and tail clonus in response to mild star-tle. This hyper-responsive behavior, which may reflect seizure activity, was not seen in *Scn1a*[RH/+] mice or WT littermates.

Although the presence of the R1648H mutation did not affect *Scn1a* transcript or protein levels, it had a significant effect on the elec-trophysiological properties of corti-cal interneurons. Increased use-de-pendent inactivation and slowed recovery from inactivation were observed in bipolar interneurons but not in pyramidal cells, and there was a decreased ratio of sodium cur-rent in bipolar to pyramidal neu-rons. The decreased sodium current is particularly noteworthy for two reasons. First, the recordings mea-sured total somatic currents, including contributions from the $Na_v1.2$ and $Na_v1.6$ isoforms, whereas the R1648H mutation should only affect $Na_v1.1$. Second, bipolar and pyramidal neurons each represent a heterogeneous group of many different types of neurons, and it is likely that $Na_v1.1$ is differ-entially expressed in many of those cell types. This heterogeneity is reflected in the large standard errors for the current density measurements in Table 1. We anticipate that the effects of the R1648H mutation will be more pronounced if examined in a homogenous population of inhib-itory neurons.

The findings from the electrophysiological analysis of the sodium channel properties in the knock-in mice are consistent with our previous analysis of cortical interneurons from BAC transgenic mice expressing the *SCN1A*-R1648H mutation (14).

indicates that these neurons have reduced excitability, consis-tent with decreased sodium channel activity.

DISCUSSION

Several characteristics of the R1648H knock-in mice are sim-ilar to the clinical features of the human GEFS+ patients, who are heterozygous for the mutation. Heterozygous *Scn1a*[RH/+] mice have normal life spans, reduced thresholds to febrile sei-zures, and spontaneous seizures. Homozygous *Scn1a*[RH/RH]

TABLE 2

Parameters of sodium channel properties from bipolar neurons

The electrophysiological properties were fit according to the equations described under "Experimental Procedures." The values shown are the mean ± S.E.

	P5-P8			P13-P15		
	RH/RH	RH/+	WT	RH/RH	RH/+	WT
Voltage dependence of activation						
Gating charge (z)	3.4 ± 0.7	3.9 ± 0.8	3.5 ± 1.2	5.9 ± 0.9	3.8 ± 0.8	5.8 ± 2.1
$V_{1/2}$ (mV)	−21.5 ± 5.1	−20.9 ± 5.8	−21.1 ± 6.2	−31.9 ± 6.4	−32.5 ± 4.3	−30.3 ± 3.3
n	5	8	3	6	4	8
Voltage dependence of inactivation						
Slope (a)	7.9 ± 2.3	9.2 ± 1.7	10.1 ± 1.1	7.2 ± 1.3	9.3 ± 2.5	7.2 ± 1.2
$V_{1/2}$ (mV)	−53.5 ± 7.3	−58.9 ± 7.2	−54.8 ± 6.9	−58.4 ± 6.3	−58.9 ± 7.3	−58.9 ± 6.1
n	5	12	5	6	5	6
Recovery from inactivation						
Ratio (a)	0.9 ± 0.23	0.9 ± 0.16	1.1 ± 0.05	0.94 ± 0.12	0.99 ± 0.11	0.95 ± 0.07
τ_1 (ms)	9.5 ± 0.5[a]	7.6 ± 0.4[a]	5.1 ± 0.3	9.6 ± 0.2[a]	10.4 ± 0.4[a]	7.6 ± 0.1
Fraction recovered	0.8 ± 0.04[a]	0.9 ± 0.06	0.95 ± 0.02	0.9 ± 0.03[a]	0.92 ± 0.04	0.94 ± 0.02
n	4	8	5	8	4	6
Use dependence at 39 Hz						
Fraction decayed (A)	0.5 ± 0.06	0.4 ± 0.04	0.4 ± 0.02	0.4 ± 0.08	0.3 ± 0.06	0.3 ± 0.03
τ_1 (s)	0.5 ± 0.03[a]	0.6 ± 0.07	0.7 ± 0.04	0.6 ± 0.08	0.5 ± 0.07[a]	0.8 ± 0.1
Remaining current (C)	0.2 ± 0.06[a]	0.4 ± 0.08	0.4 ± 0.09	0.38 ± 0.09	0.4 ± 0.08	0.5 ± 0.09
n	6	19	17	18	8	9
Use dependence at 10 Hz						
Fraction decayed (A)	0.1 ± 0.04	0.1 ± 0.04	0.1 ± 0.02	0.3 ± 0.06	0.3 ± 0.08	0.2 ± 0.09
τ_1 (s)	0.6 ± 0.1	0.7 ± 0.08[a]	0.5 ± 0.02	0.3 ± 0.07[a]	0.4 ± 0.08[a]	0.8 ± 0.09
Remaining current (C)	0.8 ± 0.02[a]	0.8 ± 0.09	0.9 ± 0.06	0.72 ± 0.09[a]	0.76 ± 0.05	0.86 ± 0.06
n	7	11	14	15	8	10
Persistent current						
Percent	0.7 ± 0.1	0.9 ± 0.2	1.0 ± 0.1	0.7 ± 0.1	0.7 ± 0.2	0.9 ± 0.3
n	6	9	11	9	6	7

[a] Statistically significant difference compared to wild-type neurons ($p < 0.05$).

TABLE 3

**Parameters of sodium channel properties from pyramidal neurons**

The electrophysiological properties were fit according to the equations described under "Experimental Procedures." The values shown are means ± S.E. of the mean.

	P5-P8			P13-P15		
	RH/RH	RH/+	WT	RH/RH	RH/+	WT
Voltage dependence of activation						
Gating charge (z)	5.0 ± 1.3	6.1 ± 1.2	4.4 ± 0.9	4.4 ± 0.9	4.9 ± 1.2	6.7 ± 0.8
$V_{1/2}$ (mV)	−27.6 ± 5.6	−26.7 ± 4.9	−24.5 ± 5.3	−30.9 ± 4.9	−31.8 ± 3.7	−32.2 ± 5.3
n	6	5	3	4	3	3
Voltage dependence of inactivation						
Slope (a)	9.0 ± 1.3	7.3 ± 2.7	8.1 ± 1.9	6.7 ± 1.5	7.0 ± 2.7	7.4 ± 1.9
$V_{1/2}$ (mV)	−56.9 ± 7.3	−56.6 ± 6.7	−52.3 ± 7.2	−58.8 ± 4.3	−55.2 ± 6.3	−55.5 ± 5.2
n	9	6	4	5	5	5
Recovery from inactivation						
Ratio (a)	0.9 ± 0.04	1.0 ± 0.07	0.8 ± 0.06	0.98 ± 0.06	0.99 ± 0.07	0.97 ± 0.06
τ_1 (ms)	8.1 ± 0.11	9.4 ± 0.08	9.4 ± 0.06	6.9 ± 0.13[a]	9.5 ± 0.07	9.3 ± 0.06
Fraction recovered	0.9 ± 0.02	0.9 ± 0.03	0.9 ± 0.03	0.9 ± 0.06	0.9 ± 0.04	0.9 ± 0.05
n	3	8	9	8	4	6
Use dependence at 39 Hz						
Fraction decayed (A)	0.5 ± 0.01	0.4 ± 0.03	0.4 ± 0.05	0.3 ± 0.01	0.3 ± 0.04	0.4 ± 0.07
τ_1 (s)	0.6 ± 0.04	0.5 ± 0.07	0.5 ± 0.04	0.4 ± 0.07	0.5 ± 0.09	0.5 ± 0.02
Remaining current (C)	0.3 ± 0.06	0.4 ± 0.09	0.4 ± 0.09	0.3 ± 0.08	0.3 ± 0.06	0.4 ± 0.06
n	5	13	17	8	4	5
Use dependence at 10 Hz						
Fraction decayed (A)	0.2 ± 0.01	0.2 ± 0.03	0.2 ± 0.04	0.2 ± 0.004	0.2 ± 0.07	0.25 ± 0.03
τ_1 (s)	0.6 ± 0.1	0.3 ± 0.05	0.3 ± 0.08	0.3 ± 0.03	0.3 ± 0.06	0.3 ± 0.02
Remaining current (C)	0.8 ± 0.08	0.8 ± 0.08	0.8 ± 0.09	0.83 ± 0.06	0.85 ± 0.02	0.81 ± 0.04
n	7	17	19	12	3	7
Persistent current						
Percent	0.9 ± 0.2	0.8 ± 0.2	0.7 ± 0.1	0.5 ± 0.1	0.9 ± 0.2	0.8 ± 0.3
n	7	7	19	10	4	6

[a] Statistically significant difference compared to wild-type neurons ($p < 0.05$).

However, we were only able to observe the effects of the mutation in the BAC transgenic mice when the mutant sodium currents were isolated by recording in the presence of saxitoxin. The fact that the mutation had comparable effects in homozygous knock-in mice demonstrates that the alterations were not due to use-dependent block by saxitoxin during recording from the BAC transgenic mice. In addition, we also observed that bipolar neurons from *Scn1a*[RH/RH] homozygous knock-in mice exhibit decreased action potential firing compared with neurons from WT or *Scn1a*[RH/+] heterozygous mice. The fact that decreased firing was observed only in bipolar and not pyramidal neurons most likely reflects greater expression of the Na$_v$1.1
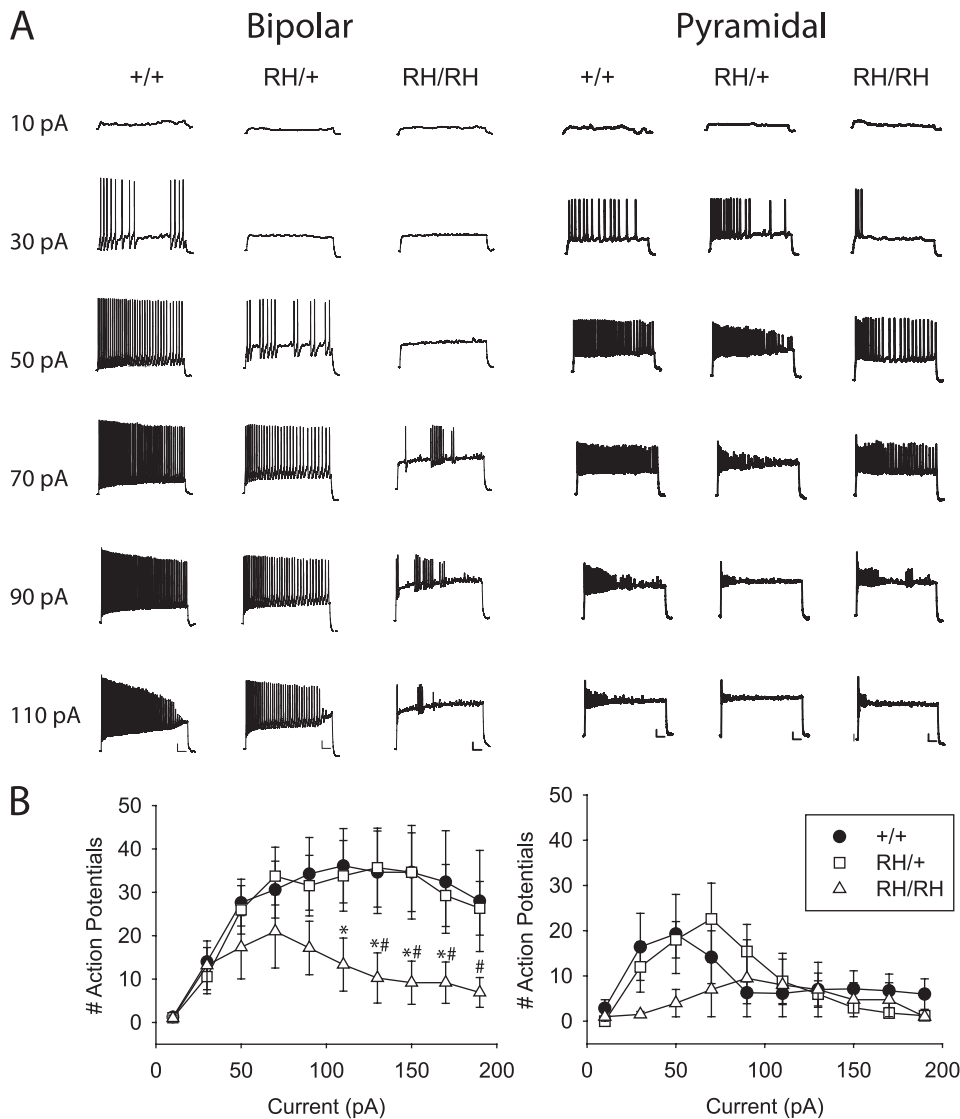
FIGURE 8. **Decreased action potential firing in dissociated cortical bipolar neurons.** *A*, firing patterns were recorded during 2-s depolarizing current injections in 20-pA increments, starting at 10 pA. *Scale bars* indicate 10 mV and 200 ms. *B*, the number of action potentials during the 2-s current injection is plotted *versus* the magnitude of the current. Sample sizes were 10 for bipolar WT, 19 for bipolar *Scn1a^RH/+^*, 12 for bipolar *Scn1a^RH/RH^*, 7 for pyramidal WT, 5 for pyramidal *Scn1a^RH/+^*, and 4 for pyramidal *Scn1a^RH/RH^*. *Symbols* represent means, and *error bars* indicate S.E. The *asterisk* (*) indicates statistically significant difference compared with WT, and the *number symbol* (#) indicates statistically significant difference compared with *Scn1a^RH/+^* ($p < 0.05$).

tonic seizure, whereas this progression was rarely seen in WT or *Scn1a^RH/+^* mice, and when evident took several minutes to occur.

In contrast to the consistent results that were observed from the analysis of cortical interneurons from the R1648H knock-in and BAC transgenic mice, differences between the models were identified from the analysis of cortical pyramidal cells. The only electrophysiological abnormalities detected in cortical pyramidal cells from the knock-in mice was slightly faster recovery from inactivation in homozygous P13-P15 mutants and a lower number of action potentials at low current injections. However, the difference in recovery was small enough so that it did not result in an increase in use-dependent inactivation, and the number of action potentials at higher levels of current was comparable with that for WT mice. In contrast, cortical pyramidal cells from the BAC transgenic mice revealed a hyperpolarizing shift in the voltage dependence of inactivation (14). The two models also differed in seizure severity and susceptibility. The knock-in mice exhibited spontaneous seizures, EEG abnormalities and normal thresholds to kainic acid-induced seizures. In contrast, BAC transgenic mice were more susceptible to kainic acid-induced seizures but did not show spontaneous seizure activity. Differences between the two models were not surprising as the BAC transgene is unlikely to fully recapitulate the temporal and spatial expression of the endogenous *Scn1a* gene, and the knock-in mice represent a more accurate disease model.

Functional studies in heterologous expression systems have failed to identify a common abnormality in *SCN1A* mutations from patients with GEFS+. In different experimental systems, biophysical analysis of the R1648H mutation in Na$_v$1.1 demonstrated either increased recovery from fast inactivation (9) or increased persistent current (10). Analysis of the comparable mutation in Na$_v$1.2 demonstrated a positive shift in the voltage dependence of inactivation (30), and analysis in Na$_v$1.4 identified a negative shift in the voltage dependence of activation and inactivation and increased recovery from fast inactivation (28). Analyses of other GEFS+ mutations in heterologous expression systems have also been difficult to interpret, with the biophysical abnormalities of some mutations being consistent with

channel in bipolar compared with pyramidal neurons, as we previously observed in the BAC transgenic mice (14) and others observed in the *Scn1a* knock-out mouse models of SMEI (15, 16).

Based on these effects, interneurons containing R1648H mutant sodium channels would be less reliable in propagating high frequency trains of action potentials, leading to a reduction in GABAergic inhibition. Given the importance of inhibitory circuits in controlling the excitability of postsynaptic neurons, it seems likely that reduced firing of cortical interneurons and possibly other GABAergic interneurons contributes to the seizure generation in the *Scn1a^R1648H^* mouse models. Reduced inhibition is also consistent with the rapid, abnormal propagation of experimental febrile seizures in these mice. Most *Scn1a^RH/RH^* mutant mice became immobile (the typical onset of experimental febrile seizure), then immediately progressed to a

increased neuronal excitability (9, 11, 31, 32) and others predicting decreased neuronal excitability (9, 12, 13). It was not known from studies in heterologous systems whether the mutations primarily affect excitatory or inhibitory neurons. Results from our analysis of the biophysical properties of the R1648H mutation in neurons from the knock-in mice suggest that the primary effect of this mutation is to delay recovery from inactivation and, thus, decrease the firing of inhibitory neurons. Impairment of inhibition could be a general effect of *SCN1A* mutations, but analyses of mouse models with other *Scn1a* mutations are needed to determine whether this is a consistent mechanism.

Studies of two complete loss-of-function mutations of *Scn1a* in mouse models of SMEI also showed diminished GABAergic interneuron function. Heterozygotes for a knock-out mutation of *Scn1a* displayed reduced $Na_v1.1$ channel expression, reduced sodium currents, and an inability to sustain repetitive firing in GABAergic interneurons of the cortex and hippocampus (15, 16). It is interesting that the R1648H homozygotes exhibit a time course of seizure initiation and progression to lethality that is very similar to the homozygous null mice, demonstrating a profound reduction of *in vivo* function as a result of this mutation. This was unexpected given the relatively small effects observed in heterologous systems. We propose that decreased excitability of the inhibitory circuitry is a major factor contributing to seizure generation in mouse models of GEFS+ and SMEI and, by extension, GEFS+ and SMEI patients. A similar mechanism may also underlie other *SCN1A*-derived disorders.

REFERENCES

1. Escayg, A., MacDonald, B. T., Meisler, M. H., Baulac, S., Huberfeld, G., An-Gourfinkel, I., Brice, A., LeGuern, E., Moulard, B., Chaigne, D., Buresi, C., and Malafosse, A. (2000) *Nat. Genet.* **24,** 343–345
2. Claes, L., Del-Favero, J., Ceulemans, B., Lagae, L., Van Broeckhoven, C., and De Jonghe, P. (2001) *Am. J. Hum. Genet.* **68,** 1327–1332
3. Vanmolkot, K. R. J., Babini, E., de Vries, B., Stam, A. H., Freilinger, T., Terwindt, G. M., Norris, L., Haan, J., Frants, R. R., Ramadan, N. M., Ferrari, M. D., Pusch, M., van den Maagdenberg, A. M. J. M., and Dichgans, M. (2007) *Hum. Mutat.* **28,** 522
4. Meisler, M. H., and Kearney, J. A. (2005) *J. Clin. Invest.* **115,** 2010–2017
5. Catterall, W. A., Dib-Hajj, S., Meisler, M. H., and Pietrobon, D. (2008) *J. Neurosci.* **28,** 11768–11777
6. Martin, M. S., Tang, B., Papale, L. A., Yu, F. H., Catterall, W. A., and Escayg, A. (2007) *Hum. Mol. Genet.* **16,** 2892–2899
7. Osaka, H., Ogiwara, I., Mazaki, E., Okamura, N., Yamashita, S., Iai, M., Yamada, M., Kurosawa, K., Iwamoto, H., Yasui-Furukori, N., Kaneko, S., Fujiwara, T., Inoue, Y., and Yamakawa, K. (2007) *Epilepsy Res.* **75,** 46–51
8. Mahoney, K., Moore, S. J., Buckley, D., Alam, M., Parfrey, P., Penney, S., Merner, N., Hodgkinson, K., and Young, T. L. (2009) *Seizure* **18,** 492–497
9. Spampanato, J., Escayg, A., Meisler, M. H., and Goldin, A. L. (2001) *J. Neurosci.* **21,** 7481–7490
10. Lossin, C., Wang, D. W., Rhodes, T. H., Vanoye, C. G., and George, A. L., Jr. (2002) *Neuron* **34,** 877–884
11. Spampanato, J., Kearney, J. A., de Haan, G., McEwen, D. P., Escayg, A., Aradi, I., MacDonald, B. T., Levin, S. I., Soltesz, I., Benna, P., Montalenti, E., Isom, L. L., Goldin, A. L., and Meisler, M. H. (2004) *J. Neurosci.* **24,** 10022–10034
12. Barela, A. J., Waddy, S. P., Lickfett, J. G., Hunter, J., Anido, A., Helmers, S. L., Goldin, A. L., and Escayg, A. (2006) *J. Neurosci.* **26,** 2714–2723
13. Lossin, C., Rhodes, T. H., Desai, R. R., Vanoye, C. G., Wang, D., Carniciu, S., Devinsky, O., and George, A. L., Jr. (2003) *J. Neurosci.* **23,** 11289–11295
14. Tang, B., Dutt, K., Papale, L., Rusconi, R., Shankar, A., Hunter, J., Tufik, S., Yu, F. H., Catterall, W. A., Mantegazza, M., Goldin, A. L., and Escayg, A. (2009) *Neurobiol. Dis.* **35,** 91–102
15. Yu, F. H., Mantegazza, M., Westenbroek, R. E., Robbins, C. A., Kalume, F., Burton, K. A., Spain, W. J., McKnight, G. S., Scheuer, T., and Catterall, W. A. (2006) *Nat. Neurosci.* **9,** 1142–1149
16. Ogiwara, I., Miyamoto, H., Morita, N., Atapour, N., Mazaki, E., Inoue, I., Takeuchi, T., Itohara, S., Yanagawa, Y., Obata, K., Furuichi, T., Hensch, T. K., and Yamakawa, K. (2007) *J. Neurosci.* **27,** 5903–5914
17. Kearney, J. A., Buchner, D. A., De Haan, G., Adamska, M., Levin, S. I., Furay, A. R., Albin, R. L., Jones, J. M., Montal, M., Stevens, M. J., Sprunger, L. K., and Meisler, M. H. (2002) *Hum. Mol. Genet.* **11,** 2765–2775
18. Chen, C., Westenbroek, R. E., Xu, X., Edwards, C. A., Sorenson, D. R., Chen, Y., McEwen, D. P., O'Malley, H. A., Bharucha, V., Meadows, L. S., Knudsen, G. A., Vilaython, A., Noebels, J. L., Saunders, T. L., Scheuer, T., Shrager, P., Catterall, W. A., and Isom, L. L. (2004) *J. Neurosci.* **24,** 4030–4042
19. Racine, R. J. (1972) *Electroencephalogr. Clin. Neurophysiol.* **32,** 281–294
20. Dube, C., Chen, K., Eghbal-Ahmadi, M., Brunson, K., Soltesz, I., and Baram, T. Z. (2000) *Ann. Neurol.* **47,** 336–344
21. Dubé, C., Vezzani, A., Behrens, M., Bartfai, T., and Baram, T. Z. (2005) *Ann. Neurol.* **57,** 152–155
22. Hilgenberg, L. G., Hoover, C. L., and Smith, M. A. (1999) *J. Neurosci.* **19,** 7384–7393
23. Li, Z., Hilgenberg, L. G., O'Dowd, D. K., and Smith, M. A. (1999) *J. Neurobiol.* **39,** 547–557
24. Fong, A. Y., Stornetta, R. L., Foley, C. M., and Potts, J. T. (2005) *J. Comp. Neurol.* **493,** 274–290
25. Graf, E. R., Zhang, X., Jin, S. X., Linhoff, M. W., and Craig, A. M. (2004) *Cell* **119,** 1013–1026
26. Schank, J. R., Liles, L. C., and Weinshenker, D. (2005) *Epilepsy Res.* **65,** 23–31
27. Martina, M., Vida, I., and Jonas, P. (2000) *Science* **287,** 295–300
28. Alekov, A., Rahman, M. M., Mitrovic, N., Lehmann-Horn, F., and Lerche, H. (2000) *J. Physiol.* **529,** 533–539
29. Naritoku, D. K., Casebeer, D. J., and Darbin, O. (2003) *Epilepsia* **44,** 912–916
30. Kühn, F. J., and Greeff, N. G. (1999) *J. Gen. Physiol.* **114,** 167–183
31. Spampanato, J., Escayg, A., Meisler, M. H., and Goldin, A. L. (2003) *Neuroscience* **116,** 37–48
32. Spampanato, J., Aradi, I., Soltesz, I., and Goldin, A. L. (2004) *J. Neurophysiol.* **91,** 2040–2050